GEOPHYSICS, VOL. 86, NO. 3 (MAY-JUNE 2021); P. V233–V244, 14 FIGS.
10.1190/GEO2020-0169.1

Robust singular value decomposition filtering for low signal-to-noise ratio seismic data

Chao Wang[1] and Yun Wang[2]

ABSTRACT

Reduced-rank filtering is a common method for attenuating noise in seismic data. Because conventional reduced-rank filtering distinguishes signals from noises only according to singular values, it performs poorly when the signal-to-noise ratio (S/N) is very low or when data contain high levels of isolate or coherent noise. Therefore, we have developed a novel and robust reduced-rank filtering method based on singular value decomposition in the time-space domain. In this method, noise is recognized and attenuated according to the characteristics of the singular values and the singular vectors. The left and right singular vectors corresponding to large singular values are selected first. Then, the right singular vectors are classified into different categories according to their curve characteristics, such as jump, pulse, and smooth. Each kind of right singular vector is related to a type of noise or seismic event, and it is corrected by using a different filtering technology, such as mean filtering, edge-preserving smoothing, or edge-preserving median filtering. The left singular vectors are also corrected by using the filtering methods based on frequency attributes such as main frequency and frequency bandwidth. To process seismic data containing a variety of events, local data are extracted along the local dip of the event. The optimal local dip is identified according to the singular values and singular vectors of the data matrices that are extracted along different trial directions. This new filtering method has been applied to synthetic and field seismic data, and its performance is compared with that of several conventional filtering methods. The results indicate that the new method is more robust for data with a low S/N, strong isolated noise, or coherent noise. The new method also overcomes the difficulties associated with selecting an optimal rank.

INTRODUCTION

Useful seismic signals are usually contaminated by various types of noise, such as ground roll, single-frequency interferences, multiples, linear noise, or Gaussian random noise. These noises can cause serious problems during seismic data processing and interpretation. Therefore, seismic signal enhancement and noise attenuation are critically important and widely used in seismic processing.

Numerous denoising techniques have been proposed to increase the signal-to-noise ratio (S/N) of seismic data. Many of these methods have been proposed in the transform domain, including bandpass filtering, f-k filtering, time-frequency peak filtering (Tian et al., 2014), and time-frequency filtering based on the wavelet transform (Gao et al., 2006) or the shearlet transform (Zhang and van der Baan, 2018). Although these methods have been effective, they cannot remove the noise energy that overlaps the signal in the transform domain, and some of these methods present difficulties in terms of selecting thresholds. Other kinds of well-known methods for seismic data denoising include adaptive filtering (Jeng et al., 2009) and adaptive prediction filtering, in either the frequency-space (Liu et al., 2012) or time-space (Liu and Li, 2018) domains. These methods can automatically adjust filtering parameters and do not require prior information on noise statistics. However, as a precondition for using these methods, the noise sequence must exhibit nonautocorrelation. Moreover, there is also the issue that noise reduction is often accompanied by signal degradation. Other widely used methods include median filtering (Huo et al., 2012), variational mode decomposition (Yu and Ma, 2018), and matched filtering (Cai

Manuscript received by the Editor 18 March 2020; revised manuscript received 25 January 2021; published ahead of production 10 March 2021; published online 21 April 2021.
[1]Chinese Academy of Sciences, Institute of Geochemistry, The State Key Laboratory of Ore Deposit Geochemistry, Guiyang 550081, China. E-mail: srmn28@163.com (corresponding author).
[2]China University of Geosciences, School of Geophysics and Information Technology, Beijing 100083, China. E-mail: yunwang@mail.iggcas.ac.cn.

and Ma, 2019). Generally, these existing methods can efficiently reduce the effect of noise when the S/N is high. Currently, the challenge is to develop more powerful denoising methods for seismic data with a low S/N (Wang et al., 2019; Zhang and van der Baan, 2019; Lin and Zhang, 2020). This is particularly relevant for microseismic signals, characterized by wide frequency bands, small magnitudes, and extremely low S/N values; these factors render it difficult to recover microseismic signals.

Reduced-rank filtering is a kind of method in which an initial data set is separated into signal and noise subspaces, based on the assumptions that seismic data are of a low-rank structure and noise increases the rank of the data matrix. These methods have excellent performance when used for multichannel seismic data denoising. Some rank-reduction methods are implemented in the frequency-space domain, including Cadzow filtering (Trickett, 2002, 2008) and multichannel singular spectrum analysis (Oropeza and Sacchi, 2011). Cadzow filtering can reconstruct several linear events with different slopes at the same time; however, it produces noticeable artifacts for isolated large-amplitude noise (erratic noise) and blurs the discontinuities of seismic events. To attenuate erratic noise, Chen and Sacchi (2015) improve the classic singular spectrum analysis method by replacing truncated singular value decomposition (SVD) with a new low-rank matrix factorization technology. To separate Gaussian random noise more thoroughly, Huang et al. (2016) introduce a damping factor into the traditional multichannel singular spectrum analysis to dampen singular values. The damped multichannel singular spectrum analysis has since been extended for 5D seismic data denoising and reconstruction. Zhang et al. (2017) combine the benefits of the sparsity-promoting transform and rank-reduction methods. Rank reduction is generally achieved by using SVD, which requires high levels of computational complexity. Therefore, Gao et al. (2013) use the Lanczos bidiagonalization algorithm rather than SVD to reduce the computation time. Subsequently, the orthogonal rank-one matrix pursuit algorithm (Jia et al., 2016) and the fast orthogonal rank-one matrix pursuit algorithm (Liu et al., 2019) have been successively adopted to replace SVD for reducing the computation time.

Reduced-rank filtering can also be implemented in the time-space domain. Freire and Ulrych (1988) are the first to apply it for separating up- and downgoing waves in vertical seismic profiling via SVD. They introduce low-pass, band-pass, and high-pass eigenimages according to the range of singular values. This eigenimage filtering technique has also been used to extract abnormal features from magnetic resonance (Haggar et al., 1989) and ground-penetrating radar imagery (Cagnoli and Ulrych, 2001). Global SVD filtering in the time-space domain requires that effective seismic events are correlated in the horizontal direction, whereas noise is uncorrelated. To overcome this limitation, Bekara and van der Baan (2007) propose a local SVD technique, in which they first extract local seismic data using a sliding window and apply dip steering to render the coherent signal horizontally aligned. Then, SVD is performed on these local data for signal enhancement. Porsani et al. (2010, 2013) use a normal moveout correction to flatten reflection events, and SVD is thereafter applied to local seismic data extracted using a sliding window. Gan et al. (2015) propose a structure-oriented SVD, which flattened seismic reflections according to their local structure.

For all of the reduced-rank filtering methods, the selection of rank is crucial and difficult. It is important to balance noise attenuation while preserving an effective signal. A small rank may damage the signal, whereas a large rank cannot effectively suppress noise. In practice, the optimal rank may vary with different local seismic data; therefore, it is difficult to determine the optimal rank for real seismic data collected under complex conditions. Some studies estimate the optimal rank using the maximum turning point of the singular value curve (Vrabie et al., 2004; Hassanpour et al., 2012); but the turning point may be difficult to determine or may not exist when the S/N is low. Cary and Zhang (2009) propose an adaptive eigenimage filtering method for ground-roll attenuation by determining the number of ranks according to the S/N. However, it is difficult to estimate the S/N when the noise is unknown. Indeed, even the rank-1 matrix corresponding to the dominant signal parts may be contaminated by noise. Moreover, sometimes signals are not even contained in the rank-1 matrix. For these reasons, Vrabie et al. (2004) use independent component analysis to further separate signals from noise in singular vectors; Hassanpour et al. (2012) and Moreau et al. (2017) apply Savitzky–Golay smoothing filtering and Wiener filtering, respectively, to enhance singular vectors before they were used to restructure the low-rank matrix.

In this paper, an improved local SVD filtering method is presented for seismic data denoising. Considering the physical meaning of SVD for seismic data, the types of noise or seismic events can be identified according to the frequency attributes and curve characteristics of the left and right singular vectors. Therefore, different filtering strategies are used to correct the singular vectors. After this processing, we can accurately reconstruct signals with more singular vectors without introducing noise, thus rendering the rank selection easier.

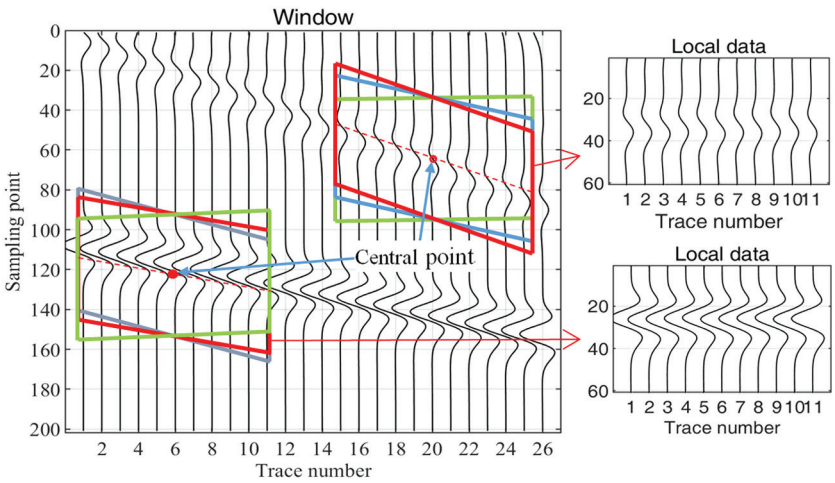

Figure 1. Illustration of dip scanning and the local data extracted using the optimal window (the red window).

METHOD

SVD

Assume that **D** is an $m \times n$ matrix; it can be transformed into a product of three matrices using SVD:

$$\mathbf{D} = \mathbf{USV}^{\mathrm{T}} = \sum_{k=1}^{R} \mathbf{u}_k \sigma_k \mathbf{v}_k^{\mathrm{T}}, \quad (1)$$

where T indicates transposition, R represents the rank of $\mathbf{D}$, $\mathbf{U}$ denotes an $m\times$ m unitary matrix, and $\mathbf{V}$ indicates an $n \times n$ unitary matrix. The column vectors of $\mathbf{U}$ and $\mathbf{V}$ are $\mathbf{u}_k$ and $\mathbf{v}_k$, and they are known as the left and right singular vectors, respectively. The term $\mathbf{S}$ represents a diagonal $m \times n$ matrix, and the elements σ_k on the diagonal of $\mathbf{S}$ are called singular values. Singular values are typically sorted in decreasing order $\sigma_1 \geq \sigma_2 \geq \ldots \geq \sigma_R$. The singular vectors corresponding to large singular values contain the main information in matrix $\mathbf{D}$. When $\mathbf{D}$ represents seismic data consisting of n traces and m ($m > n$) time samples per trace, singular vectors have a definite physical meaning. Each left singular vector $\mathbf{u}_k$ represents a normalized wavelet, and its corresponding right singular vector $\mathbf{v}_k$ gives the wavelet amplitude distribution on the n traces.

Local dip scanning and data extraction

To apply SVD filtering to real seismic data, local seismic data are usually extracted with a rectangular window, and then the dipping event in this windowed data is flattened using the dip steering algorithm (Bekara and van der Baan, 2007; Gan et al., 2015). This process leads to edge artifacts. In the work described here, we extracted local seismic data with a parallelogram window, which had two sides parallel to the dip direction of the local event. Assuming that the center point of the current local data is $d(t, x)$, the local dip at this point is preestimated using a dip scanning strategy. First, M trial dips are given as follows:

$$\theta_i = \frac{i \times (\theta_{\max} - \theta_{\min})}{M} + \theta_{\min} \quad (i = 1, \ldots, M), \quad (2)$$

where $\theta_{\max}$ (sample/trace) indicates the maximum dip angle and $\theta_{\min}$ indicates the minimum dip angle. The term M represents the number of trial dips and determines the scanning accuracy level.

For each trial dip, a local seismic data set of n traces and m time samples can be extracted:

$$\mathbf{D}(\theta_i) = \begin{bmatrix} d(t-m'-n'\theta_i, x-n') & \ldots & d(t-m', x) & \ldots & d(t-m'+n'\theta_i, x+n') \\ \vdots & & \vdots & & \vdots \\ d(t-n'\theta_i, x-n') & \ldots & d(t, x) & \ldots & d(t+n'\theta_i, x+n') \\ \vdots & & \vdots & & \vdots \\ d(t+m'-n'\theta_i, x-n') & \ldots & d(t+m', x) & \ldots & d(t+m'+n'\theta_i, x+n') \end{bmatrix}, \quad (3)$$

where $m' = (m-1)/2$ and $n' = (n-1)/2$ are the widths of the half window. To facilitate filtering, m and n are odd numbers. The singular values of matrix $\mathbf{D}(\theta_i)$ are computed, and the first (largest) singular value σ_1^i is recorded. Then, the M first-singular values are compared, and the optimal local dip at data point $d(t, x)$ corresponds to the largest first-singular value $\max(\sigma_1^i, i = 1, \cdots, M)$. Local seismic data extracted along the optimal local dip are composed of horizontal events. In this process, we can further identify this optimal local dip according to the frequency attributes of the left singular vectors and the curve characteristics of the right singular vectors. A simple example of dip scanning is shown in Figure 1. The window sizes are $m = 60$ and $n = 11$. There are three trial windows for each central point: green, blue, and red. The red window is the best because it is parallel to the local event. Local data are extracted with the red window and can be seen on the right of Figure 1.

Singular vector filtering

The seismic events in the windowed data are horizontally aligned to ensure that the data matrix can be divided into the signal subspace and the noise subspace using SVD. In conventional SVD filtering, the singular value is the only criterion used to identify signal and noise, under the assumption that a large singular value relates to a

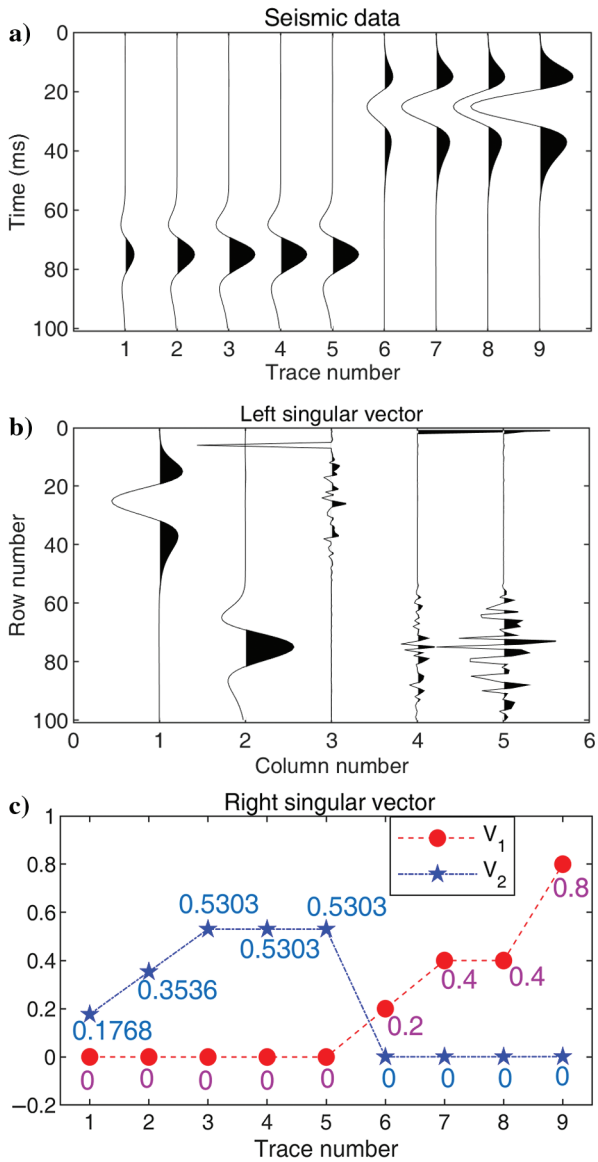

Figure 2. Example of SVD as applied to (a) synthetic seismic data. (b) The first five left singular vectors and (c) the first two right singular vectors.

trace-to-trace correlated seismic event, whereas a small singular value relates to random noise. Seismic events can therefore be reconstructed using the first K singular vectors that correspond to the first K largest singular values as follows:

$$\mathbf{D} = \sum_{k=1}^{K} \mathbf{u}_k \sigma_k \mathbf{v}_k^{\mathrm{T}}. \tag{4}$$

The selection of parameter K is difficult. A very small K cannot reconstruct the signals perfectly, whereas a large K introduces more noise. In most applications, K is set to a constant value of either 1 or 2. But in practice, the optimal value of K may vary with different local seismic data. The optimal value of K is 0 when the windowed data only contain noise, it is 1 when the windowed data contain one dip component, and it is 2 when the phase of the event varies along the x-axis or when the event is discontinuous. A larger K may also be required for data that are more complicated. Therefore, it is difficult to determine the best rank for real seismic data.

As mentioned above, a left singular vector $\mathbf{u}_k$ represents a normalized wavelet, and the corresponding right singular vector $\mathbf{v}_k$ provides the amplitude distribution of this wavelet. A typical example of SVD for synthetic seismic data is depicted in Figure 2. The input data contain two events, as shown in Figure 2a. The seismic wavelets in the first event exhibit the same shape but different maximum amplitudes, which are [0 0 0 0 0 2 4 4 8] (absolute value). The seismic wavelets in the second event also exhibit the same shape but different maximum amplitudes, which are [1 2 3 3 3 0 0 0 0]. Thus, there are two effective left singular vectors in Figure 2b. The first left singular vector represents the normalized wavelet basis of the first event, whereas the second left singular vector represents the normalized wavelet basis of the second event. The first and second right singular vectors are [0 0 0 0 0 0.2 0.4 0.4 0.8] and [0.1768 0.3536 0.5303 0.5303 0.5303 0 0 0 0], which are equal to the normalized vectors of the maximum amplitudes of the first and second events, respectively. It can be seen that a right singular vector provides the relative amplitude relationship of the wavelets in an event. When a singular vector is related to a real seismic event, it should have some characteristics similar to those of the seismic event — for instance, the amplitude of the wavelet should change slowly throughout the event. These characteristics of singular vectors also can be used to distinguish signals from noises, and several such examples have been illustrated in Figure 3. The first row in Figure 3 shows the most common case in which data (Figure 3a) contain a single event. Thus, only the first right singular vector (in Figure 3c) is stationary, whereas the other right singular vectors have random values. The second row shows a discontinuous data scenario (Figure 3d); correspondingly, we can see that one of its right singular vectors has a discontinuous jump (Figure 3f). The data shown in the third row (Figure 3g) contain an isolated noisy trace (erratic noise); because this trace exhibits strong energy, we can clearly observe that the first left singular vector represents this noise (Figure 3h). Consequently, the singular value corresponding to this erratic noise has a maximum value. This erratic noise cannot be removed according to the singular value criterion; however, it can be identified and removed according to the first right singular vector that contains a pulse (in Figure 3i). The right singular vector of coherent noise may have a curve characteristic similar to that of an effective signal. As illustrated in Figure 4, the seismic data contain two intersecting events, with the dip event being a ground roll and the horizontal event being a body wave. Here, we want to remove the low-frequency ground-roll noise. All of the first five right singular vectors are smooth (Figure 4c); however, we can distinguish ground-roll noise according to the left singular vectors (Figure 4b) because the dominant frequencies of the left singular vectors are quite different than those of the effective signal, with the exception of the third left singular vector (Figure 4d). Based on Figures 3 and 4, we can observe that even the left singular vectors corresponding to the dominant signal parts have been contaminated by noise.

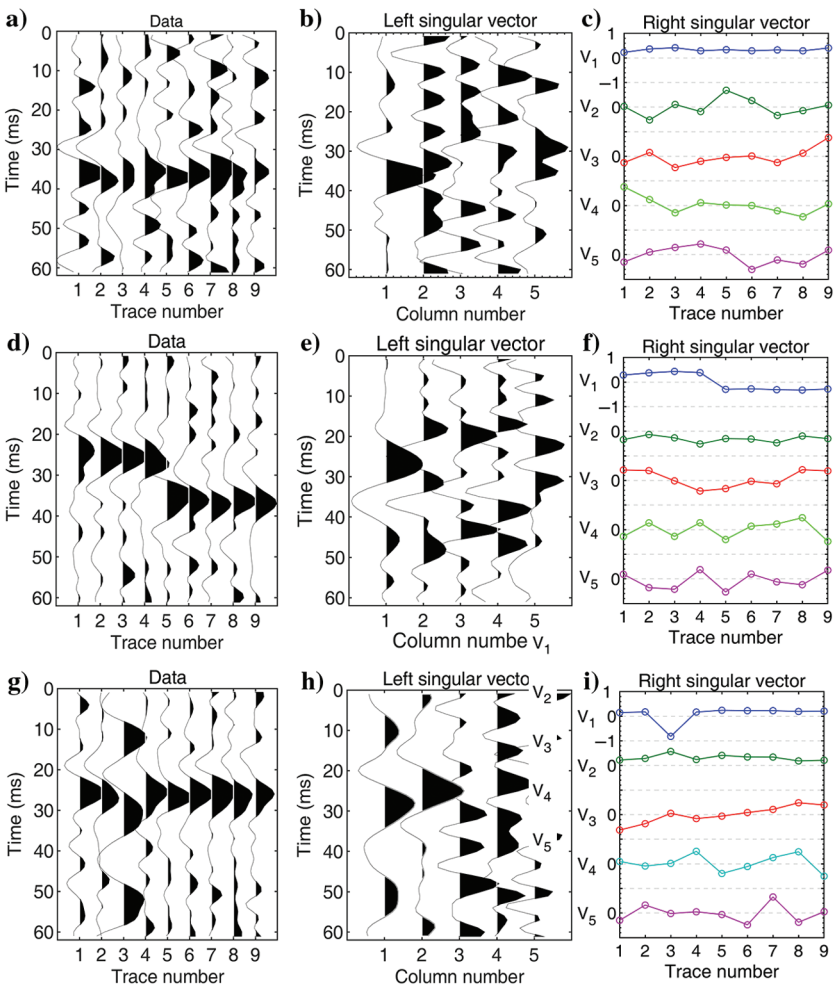

Figure 3. (a, d, and g) Three seismic data sets containing different noise, (b, e, and h) the corresponding left singular vectors (only the first five vectors are shown), and (c, f, and i) the corresponding right singular vectors.

Therefore, in our new approach, we proposed to remove noise by using the characteristics of the singular values and the singular vectors simultaneously. We first selected the K largest singular values. It is worth mentioning that the selection of rank number K is more flexible in our method, and we usually use a larger K than that used in conventional SVD filtering. Subsequently, the K right singular vectors corresponding to the K largest singular values are corrected using different methods according to their curve characteristics. In this paper, we present a simple strategy for identifying the curve characteristic of a right singular vector. When the right singular vector contains a jump, it will be filtered by using edge-preserving smoothing (EPS) (AlBinHassan et al., 2006). When the right singular vector contains large pulses, the pulses are first replaced with the median values of their neighborhoods, and then the vector is smoothed via mean filtering. As for other types of right singular vectors, they are directly corrected by using mean filtering.

It is important to note that we did not know the type of each right singular vector $\mathbf{v}$ that may contain a jump, a pulse, Gaussian random noise, or all of the above. Figure 5 shows three cases. In this method, we identify the right singular vectors according to their curve characteristics and correct them using different filtering methods.

We first determine whether the right singular vector contains pulses as follows:

First, edge-preserving median filtering (EPMF) is performed on right singular vector $\mathbf{v}$:

$$\bar{\mathbf{v}} = \mathrm{EPMF}(\mathbf{v}), \tag{5}$$

where EPMF, which can remove impulsive noise and preserve the jump, as represented by $\bar{\mathbf{v}}$ in Figure 5.

We then calculate the difference between the original vector $\mathbf{v}$ and filtered vector $\bar{\mathbf{v}}$:

$$\nabla\mathbf{v} = \mathrm{abs}(\mathbf{v} - \bar{\mathbf{v}}). \tag{6}$$

If the right singular vector contains a pulse, the difference is large at the pulse point, as represented by $\nabla\mathbf{v}$ in Figure 5a. When the right singular vector corresponds to Gaussian noise, $\nabla\mathbf{v}$ may have some large elements, but the average value is also large. We therefore divide vector $\nabla\mathbf{v}$ by its mean value: A small constant can be added to the denominator to avoid the zero value. As shown in Figure 5, $\hat{\mathbf{v}}$ has a large value at the pulse point and a small value at other points. If $\hat{v}_i (i = 1, \cdots, n)$ is greater than the given threshold α, then the ith element of vector $\mathbf{v}$ is a pulse and will be replaced with the median value of its neighborhood:

$$v_i' = \begin{cases} \bar{v}_i & \text{if } \hat{v}_i > \alpha. \\ v_i & \text{else.} \end{cases} \tag{8}$$

In this way, if the right singular vector corresponds to erratic noise, the impulsive noise in this vector is removed, as represented by $\mathbf{v}'$ in Figure 5a. No changes have been made to other types of right singular vectors, as represented by $\mathbf{v}'$ in Figure 5b and 5c.

Subsequently, we determine whether the right singular vector contains jumps as follows:

First, EPS is performed on vector $\mathbf{v}'$:

$$\bar{\mathbf{v}}' = \mathrm{EPS}(\mathbf{v}'). \tag{9}$$

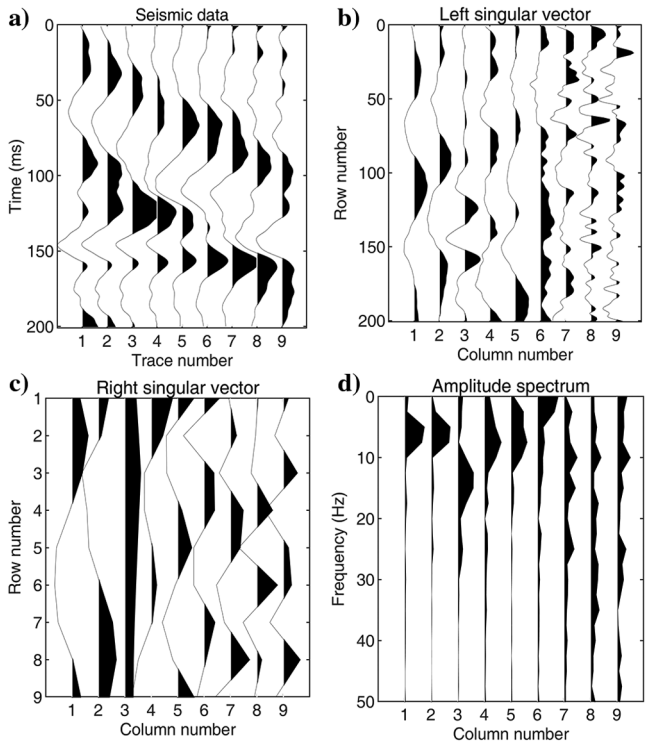

Figure 4. (a) Small matrix of seismic data, (b and c) the left and right SVD singular vectors, respectively, and (d) amplitude spectra of the left singular vectors.

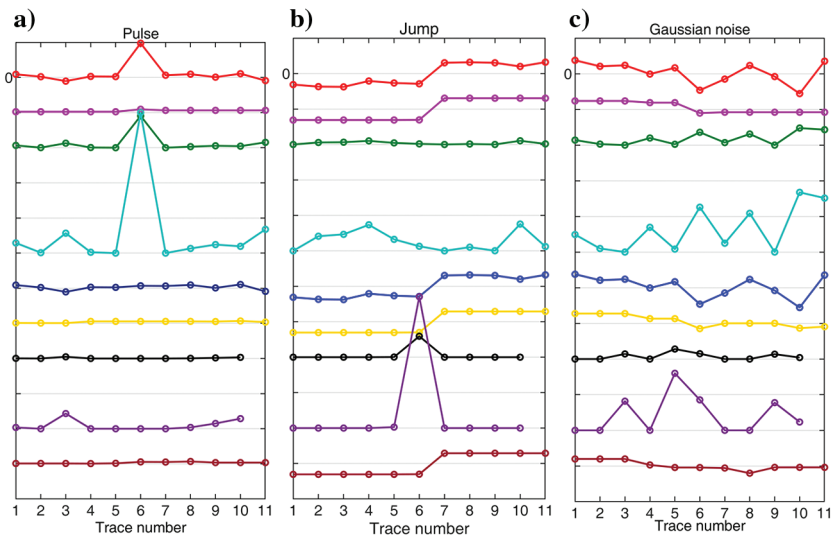

Figure 5. Schematic of the filtering processes for the right singular vector. The term $\mathbf{v}$ indicates the original right singular vector. The terms $\bar{\mathbf{v}}$, $\nabla\mathbf{v}$, and $\hat{\mathbf{v}}$ are auxiliary vectors for identifying pulses, whereas $\mathbf{v}'$ represents the right singular vector after eliminating the pulses. The terms $\bar{\mathbf{v}}'$, $\partial\bar{\mathbf{v}}'$, and $\hat{\mathbf{v}}'$ denote auxiliary vectors for identifying jumps, whereas $\mathbf{v}''$ denotes the final filtering result of the right singular vector.

We then compute the difference sequence by calculating the differences between adjacent elements of $\bar{\mathbf{v}}'$:

$$\partial\bar{\mathbf{v}}' = (\partial\bar{v}_i')_{i=1}^{n-1} = \mathrm{abs}(\bar{v}_{i+1}' - \bar{v}_i')_{i=1}^{n-1}. \tag{10}$$

When there is a jump in the right singular vector, the difference vector $\bar{\mathbf{v}}'$ has a large element at the jump point, as shown by $\partial\bar{\mathbf{v}}'$ in Figure 5b. Otherwise, all of the elements in the difference vector will be very small.

To eliminate the interference of Gaussian noise, divide vector $\partial\bar{\mathbf{v}}'$ by its mean:

$$\hat{\mathbf{v}}' \frac{\partial\bar{\mathbf{v}}'}{\mathrm{mean}(\partial\bar{\mathbf{v}}')}. \tag{11}$$

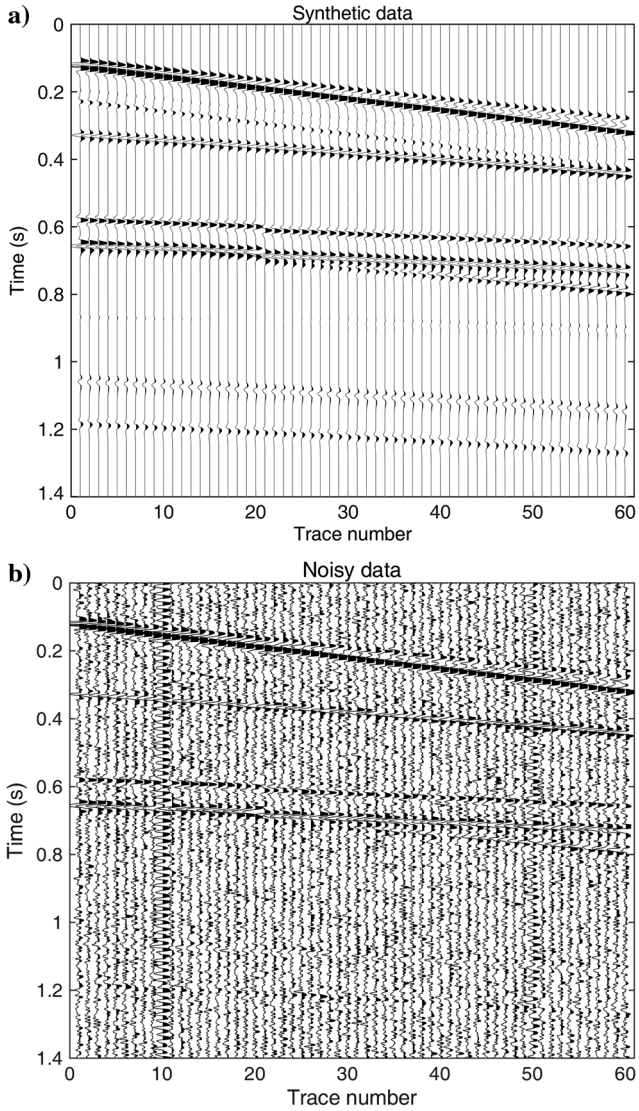

Figure 6. Synthetic seismic data (a) before and (b) after adding noise.

If at least one element in vector $\hat{\mathbf{v}}'$ is greater than a threshold β, the right singular vector $\mathbf{v}'$ is considered to contain jumps and will be filtered by EPS:

$$\mathbf{v}'' = \mathrm{EPS}(\mathbf{v}'). \tag{12}$$

Otherwise, the right singular vector $\mathbf{v}'$ is smoothed by mean filtering. From Figure 5, we can see that only the right singular vector containing jumps is filtered by EPS.

In all of the above steps, the idea of mean filtering is to replace each element value v_i with the average value over a neighborhood centered at the ith element. Mean filtering may blur the jumps. The idea of EPS is to first find the most homogeneous neighborhood of the ith element and then replace the ith element with the average value of the selected neighborhood (AlBinHassan et al., 2006). For a window of length three, there are three neighborhoods for the ith element, as follows: $(i-2, i-1, i)$, $(i-1, i, i+1)$, and $(i, i+1, i+2)$. We calculate the standard deviations for the three neighborhoods, and that with the minimum standard deviation represents the most homogeneous neighborhood. EPS is not suitable for impulsive noise. Therefore, we introduce EPMF, which is similar to EPS, but it replaces the ith element with the median value of the most homogeneous neighborhood. For seismic data denoising, the length of the right singular vector is often small; thus, the window length is set to three or at most five.

For the first K left singular vectors $\mathbf{u}_k$, various conventional filtering methods are available, and one or more can be selected according to the specific application. The filtering methods used in our study included single-frequency filtering, band-pass filtering, and main-frequency filtering. The idea of main-frequency filtering is to set the left singular vector to zero when its main frequency falls outside a given range; otherwise, it remains unchanged. For example, when attenuating ground roll, the left singular vector whose main frequency is lower than 8 Hz represents the ground roll and thus needs to be set to zero.

Finally, the effective seismic events can be reconstructed from the filtered singular vectors:

$$\mathbf{D} = \sum_{k=1}^{K} \mathbf{u}''_k \sigma_k \mathbf{v}''^{\mathrm{T}}_k. \tag{13}$$

where $\mathbf{u}''$ represents the filtered left singular vector and $\mathbf{v}''$ indicates the filtered right singular vector.

EXAMPLES

Test using synthetic data

The improved SVD filtering method was first tested on synthetic seismic data to demonstrate its effectiveness. Figure 6a shows the synthetic 2D seismic data derived using the reflectivity method. These data contain curved events, conflicting events, and discontinuities. The amplitudes of the seismic waves for different events differ and change laterally throughout the events. The data are contaminated by low-passed (0–120 Hz) Gaussian white noise, and the 10th and 50th traces are additionally affected by the 50 Hz power frequency noise (erratic noise), as shown in Figure 6b. The S/N for the noisy data shifts from low to high, with some events completely submerged in noise.

Conventional SVD filtering was first applied to the noisy data, using window parameters set to $n = 9$ traces and $m = 91$ time sam-

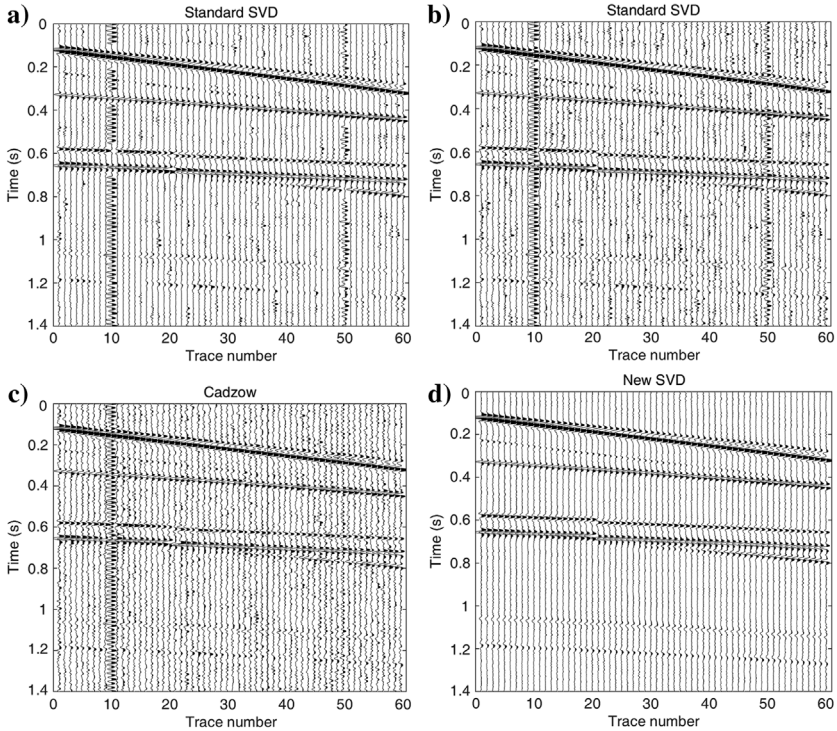

Figure 7. Filtered results achieved using conventional SVD filtering with (a) $K = 1$ and (b) $K = 2$, (c) Cadzow filtering, and (d) improved SVD filtering.

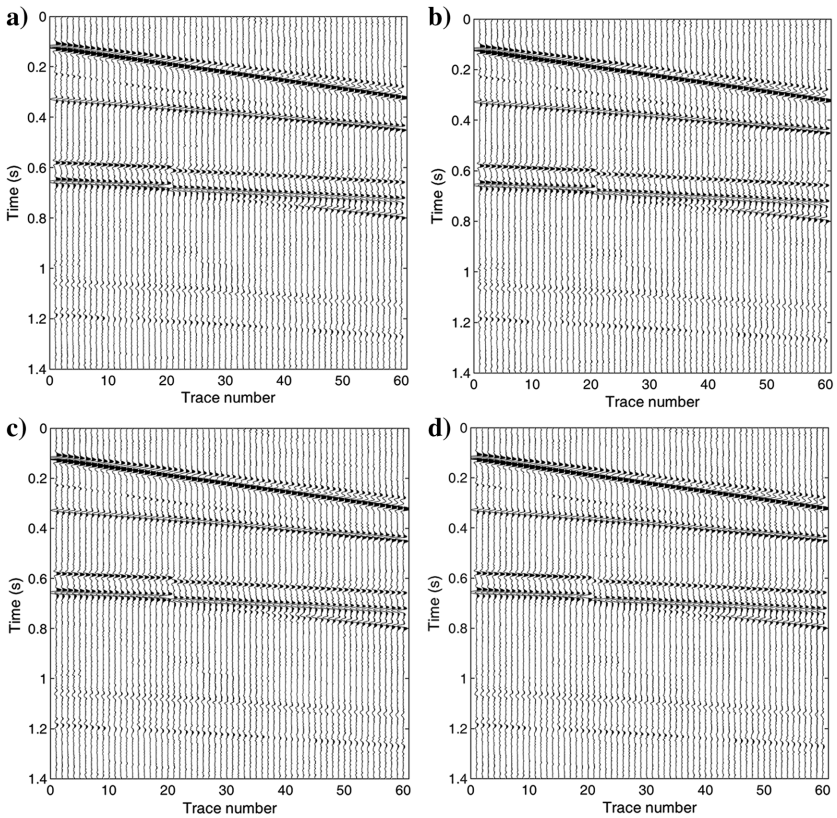

Figure 8. Filtered results of improved SVD filtering for various ranks (K) and thresholds (α and β): (a) $K = 2$, $\alpha = 3$, $\beta = 2$; (b) $K = 4$, $\alpha = 3$, $\beta = 2$; (c) $K = 3$, $\alpha = 2.5$, $\beta = 2.5$; and (d) $K = 3$, $\alpha = 2$, $\beta = 3$.

ples. The dip-scanning value ranged from −1 to 5 (sample/trace) with an interval of 0.5. The result of using only the first singular value ($K = 1$) and singular vector to reconstruct the seismic data is shown in Figure 7a. Erratic noise is not removed, and some random noises still exist in the area without seismic signals. Noticeable artifacts appear near discontinuities and weak events are only partially recovered. We then set $K = 2$, and the corresponding reconstructed data are shown in Figure 7b. The retrieved discontinuity is now clear and distinguishable; although, it also retains more noise, and weak events are still discontinuous. Based on Figure 7a and 7b, we observe that erratic noise could not be effectively removed according to the singular value. For the local data between the sixth and fourteenth traces, and 0.6 and 0.7 s, the largest singular value corresponds to the signal. However, for the local data between the sixth and fourteenth trace, 1.15 and 1.25 s, the largest singular value corresponds to noise. We then apply Cadzow filtering, with a rank of 2 and a frequency band of 0–120 Hz, to the noisy data. The filtered results can be seen in Figure 7c. We can see that the discontinuity is blurred; the large erratic noise has not been removed, and there is still considerable random noise.

Finally, the noisy data were filtered using the improved SVD filtering method. Low-pass filtering (0–120 Hz) was selected for the left singular vectors, K was set to 3, and threshold parameters α and β were set to 3 and 2, respectively. The other parameters were the same as those used in conventional SVD filtering. The filtered results are shown in Figure 7d, where we can see that the Gaussian noise has been attenuated and the erratic noise has been successfully removed according to the characteristics of the right singular vectors. Weak events and discontinuities have been properly recovered.

The filtered results obtained from the improved SVD filtering, for $K = 2$ and 4, are shown in Figure 8a and 8b, where the differences between the results for $K = 2$, 3, and 4 are very small. The average energies of the noises retained in the results for $K = 2$, 3, and 4 are 0.0131, 0.0153, and 0.0172, respectively, whereas the average energy of the initial noise is 0.1584. The random noise retained in Figure 8b ($K = 4$) is slightly stronger than that in Figure 8a ($K = 2$), indicating that the improved SVD filtering method is not particularly sensitive to parameter K. When considering $K = 3$ and changing the threshold parameters α and β, we can see the results for thresholds $\alpha = 2.5$ and $\beta = 2.5$ in Figure 8c, and for $\alpha = 2$ and $\beta = 3$ in Figure 8d. There are only slight differences between Figure 8c and 8d, and Figure 7d; the S/Ns for the

last event of these three figures are 15.93, 15.66, and 16.02 dB, respectively, thereby indicating that the improved SVD filtering method is not sensitive to threshold parameters.

The synthetic example in Figure 9 shows the edge-preserving ability of the improved SVD filtering method more clearly; here, synthetic seismic data are noiseless and contain discontinuities (Figure 9a). Figure 9b shows the filtered result of Cadzow filtering with a rank of four. It can be seen that Cadzow filtering blurs the discontinuities. Figure 9c shows the filtered result achieved using the improved SVD filtering, and it illustrates that the edges of the discontinuities are perfectly preserved by using the improved method.

Field data examples

To illustrate how the improved SVD filtering method performs in practice, we applied it to two field data sets, and the filtered results were compared with those of conventional SVD and Cadzow filtering. The improved SVD filtering method uses smooth filtering to correct the right singular vectors in the SVD domain; therefore, we also compared its performance with multidirectional median filtering (Huo et al., 2012) that directly applies median filtering to seismic data along the local dip.

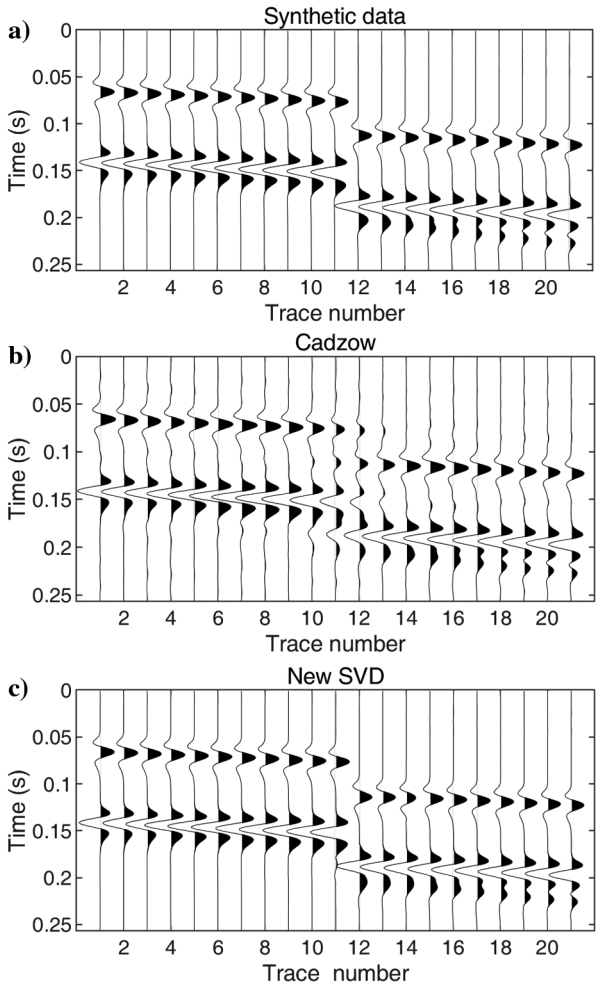

Figure 9. (a) Synthetic seismic data, (b) results after filtering using the Cadzow method, and (c) results after filtering using the improved SVD method.

Figure 10a shows the first field data that contain coherent ground-roll interference, erratic noise, and other random noise. The 65th trace data appeared to have been lost. The parameters common to each of the SVD-based filtering methods were as follows: The window parameters were set to $n = 11$ traces, $m = 201$ time samples, and dip-scanning ranged from -1 to 12 (sample/trace) with an interval of 0.5. Figure 10b shows the denoised data achieved using conventional SVD filtering with $K = 1$; it can be seen that although most of the ground roll has been removed by limiting the dip-scanning range, considerable ground-roll energy still remains at small offsets. The conventional SVD filtering method also failed to remove high-amplitude erratic noise.

For the improved SVD filtering method, K was set to 3, and threshold parameters α and β were set to 3 and 2, respectively. The main frequency filtering method (10–60 Hz) was used for the left singular vectors. Filtered data are presented in Figure 10c, where the ground roll, erratic noise, and other random noises have been suppressed. Remarkably, the lost 65th trace was retrieved by the improved SVD filtering. Multidirectional median filtering was able to remove ground roll and erratic noise, as shown in Figure 10d. However, the result of multidirectional median filtering contains more Gaussian random noise than the result of improved SVD filtering. This phenomenon can be seen more clearly from their amplitude spectra (Figure 12), where the amplitude spectrum of the result of multidirectional median filtering is larger than that of the result of improved SVD filtering at high frequencies (30–100 Hz). Cadzow filtering was implemented twice: first, with a frequency band of 0–10 Hz to attenuate the ground roll and then with a frequency band of 0–90 Hz to attenuate random noise. It can be seen that the filtered data (Figure 10e) still contain ground-roll energy at small offsets.

Figure 11a presents the differences between the original field data and the filtered result achieved using the improved SVD filtering method, in which the signal energy is not found in the noise section. The low-frequency component (0–10 Hz) of the filtered result achieved with the improved SVD filtering is shown in Figure 11b (magnified two times), where it can be seen that low-frequency component of the body waves has been well preserved. If high-pass filtering is used to suppress ground roll, the low-frequency component of body waves will be removed altogether. The average amplitude spectra for the original data and the denoised results are shown in Figure 12, where we can see that application of improved SVD filtering successfully suppressed random noise and ground roll, while preserving the signal frequency bandwidth.

The second field data set was a microseismic data set recorded in a deep well, as shown in Figure 13. The S/N of these data was very low, and low-frequency background noise was present. Here, we compared the results achieved using conventional SVD filtering, multidirectional median filtering, and improved SVD filtering. The parameters common to each of the SVD-based filtering methods were as follows: Windows were set to $n = 9$ traces and $m = 131$ time samples; dip-scanning ranged from -9 to -2 (samples/trace) and from 2 to 9 (samples/trace); and the number of singular values was selected as $K = 1$ and $K = 4$, for the

conventional and improved SVD filtering, respectively. Finally, main frequency filtering (30–150 Hz) was selected for the left singular vectors. The results achieved by applying the three filtering techniques are shown in Figure 14a–14c, where it is quite apparent that the improved SVD filtering method performed best with this field data set. The average energy of the remaining noise is 0.1725 for the conventional SVD filtering, it is 0.1184 for the multidirectional median filtering, and it is 0.0245 for the improved SVD filtering. The filtering ability of the conventional SVD method was greatly reduced by the influence of erratic noise. Multidirectional median filtering could not remove the low-frequency background noise, and some artificial events were present in the filtered section.

The noise eliminated by the three methods is shown in Figure 14d–14f, where it is evident that the improved SVD filtering method removed more noise than the other two methods. We cannot observe effective signals in the differences section of the improved SVD filtering, but we can detect minor signal energy leakage in the difference sections of the other two methods.

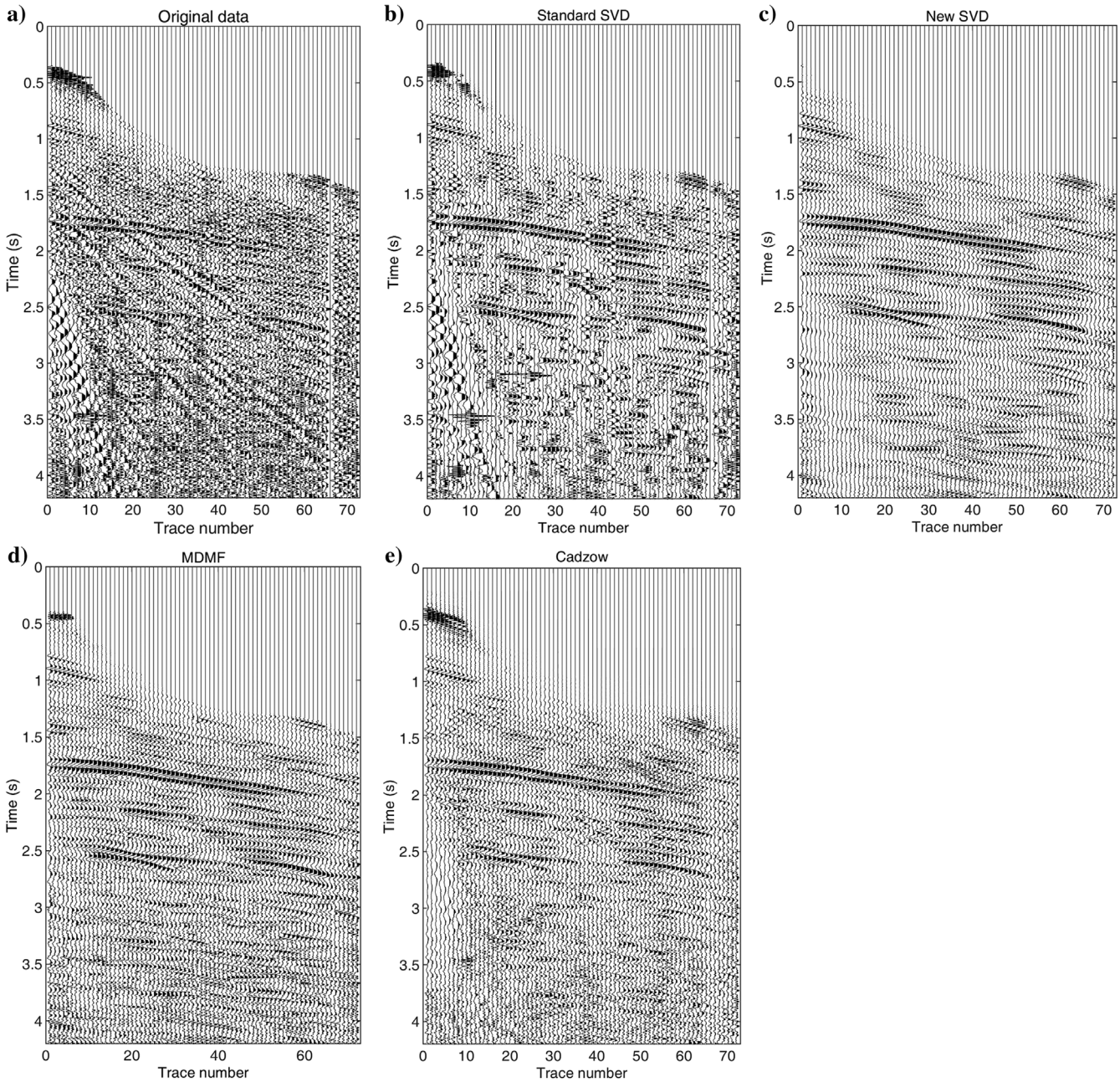

Figure 10. (a) Original field data set and filtering results achieved when using (b) conventional SVD filtering, (c) improved SVD filtering, (d) multidirectional median filtering, and (e) Cadzow filtering methods.

DISCUSSION

The examples have shown that to fully reconstruct the effective signal, the new SVD filtering method often worked best when a slightly larger K was applied. Even if the Kth eigenimage was not an effective signal, it would only result in a small amount of noise because when the Kth eigenimage corresponded to random noise, the elements of the Kth right singular vector had very small values after smoothing. When the Kth eigenimage corresponded to coherent noise, the Kth left singular vector was zeroed.

From the filtering process of the right singular vectors, we know that the threshold parameters α and β determine the type of filtering method used for a right singular vector. In any case, one of mean filtering, EPS, and EPMF will be used. In practical applications, only a few experiments are required to obtain good threshold parameters. We only need to ensure that most of the right singular vectors are correctly recognized and filtered; even if a few right singular vectors with fuzzy features are misclassified, it will not have much impact on the filtered seismic data. For example, a right singular vector containing a small jump was classified as that containing Gaussian noise, which led it to be smoothed by mean filtering; however, because the jump was small, the differences between the results achieved by mean filtering and EPS were very small. Therefore, the new SVD filter-

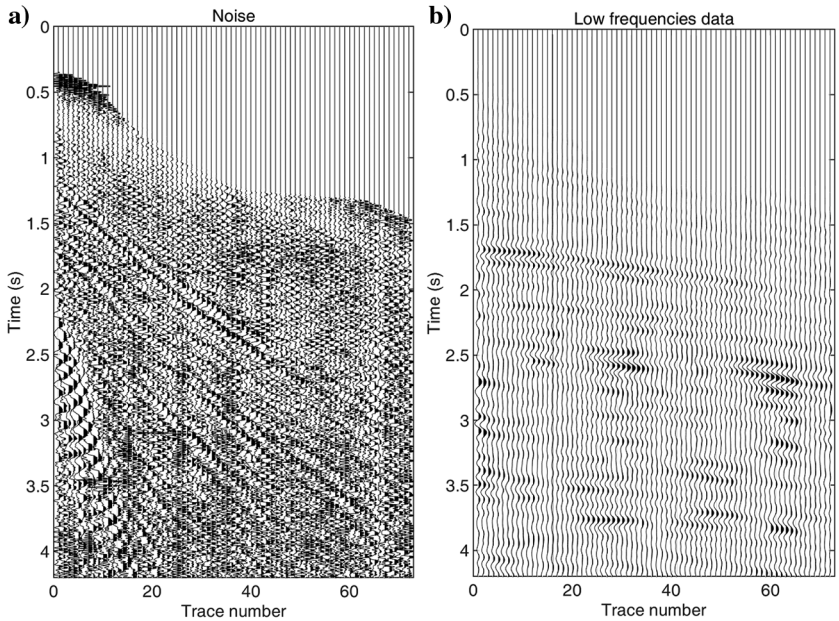

Figure 11. (a) Difference between the original data and the results achieved by applying improved SVD filtering. (b) Low-frequency component of the results achieved by applying improved SVD filtering.

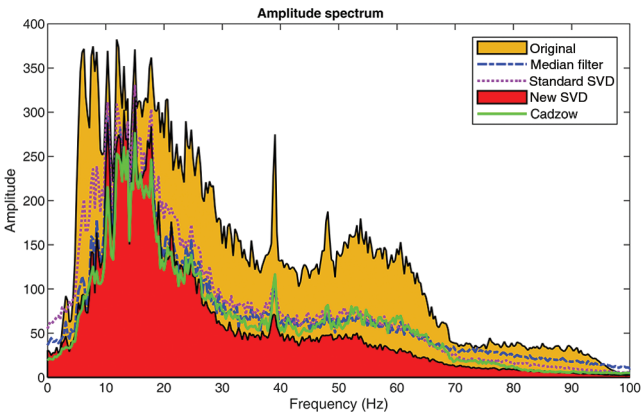

Figure 12. Average amplitude spectrums for the original data (yellow), and the data filtered using multidirectional median filtering (blue), conventional SVD filtering (purple), improved SVD filtering (red), and Cadzow filtering (green).

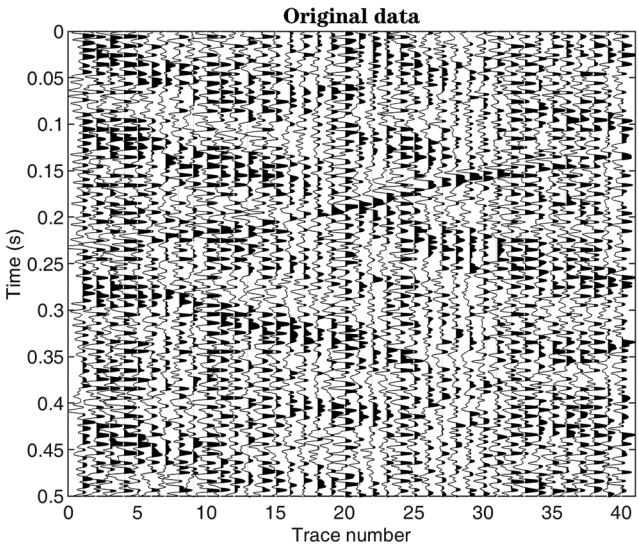

Figure 13. Original microseismic data.

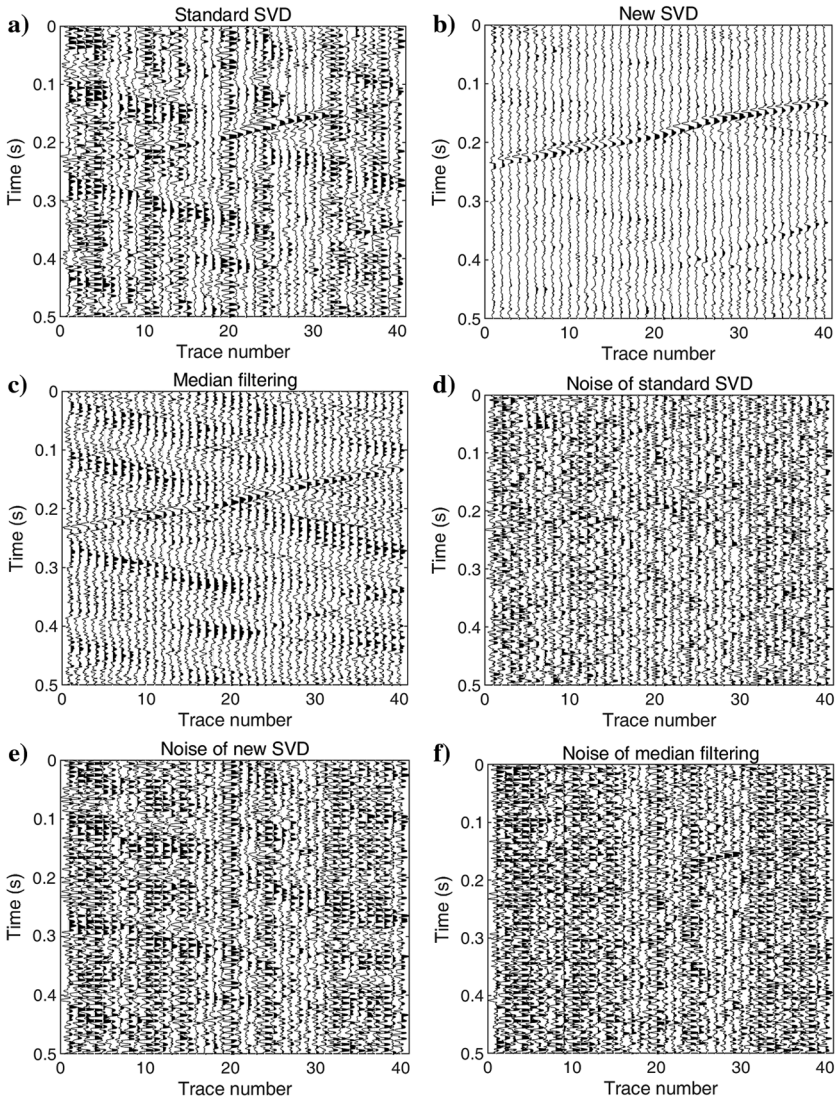

Figure 14. Filtered results achieved using (a) conventional SVD filtering, (b) improved SVD filtering, and (c) multidirectional median filtering. Differences between the original microseismic data and the filtered data achieved using (d) conventional SVD filtering, (e) improved SVD filtering, and (f) multidirectional median filtering.

ing method is not highly sensitive to the threshold parameters α and β.

CONCLUSION

We have introduced a new method for attenuating the noise of seismic data in the SVD domain. Based on the physical meaning of SVD, the right singular vectors corresponding to erratic noise, Gaussian random noise, and continuous and discontinuous seismic events have different curve characteristics, such as pulse, random, smooth, and jump. Therefore, the right singular vectors are used to attenuate noise by correcting them with mean filtering, EPS or EPMF. The left singular vectors are also used to identify and attenuate noise according to their attributes such as main frequency and frequency bandwidth. When noise is so strong that its corresponding singular value is greater than that of the signal, it can still be attenuated by this new SVD filtering. The denoising effect of the new SVD filtering method does not strictly depend on rank selection; therefore, we can select more singular vectors than those selected using the classic reduced-rank filtering to ensure that effective seismic events are accurately reconstructed. Although the new method requires using two more threshold parameters, it is not highly sensitive to these parameters, and only a few experiments are needed to obtain the good threshold parameters. Examples show that our new SVD filtering method is more robust than conventional SVD filtering, Cadzow filtering, and multidirectional median filtering, and it has the ability to remove strong Gaussian noise, large-amplitude erratic noise, and coherent noise. The new method can also be used to separate different wavefields by limiting the local dip scanning range, for example, to separate up- and downgoing waves.

ACKNOWLEDGMENTS

This research was funded by the National Key Research and Development Project (2018YFC1503705) and the National Natural Science Foundation of China (grant nos. 41874166, U1839208, and 41504107).

DATA AND MATERIALS AVAILABILITY

Data associated with this research are confidential and cannot be released.

REFERENCES

AlBinHassan, N. M., Y. Luo, and M. N. Al-Faraj, 2006, 3D edge-preserving smoothing and applications: Geophysics, **71**, no. 4, P5–P11, doi: 10.1190/1.2213050.

Bekara, M., and M. van der Baan, 2007, Local singular value decomposition for signal enhancement of seismic data: Geophysics, **72**, no. 2, V59–V65, doi: 10.1190/1.2435967.

Cagnoli, B., and T. J. Ulrych, 2001, Singular value decomposition and wavy reflections in ground-penetrating radar images of base surge deposits: Journal of Applied Geophysics, **48**, 175–182, doi: 10.1016/S0926-9851(01)00089-1.

Cai, K. J., and J. W. Ma, 2019, Robust estimation of multiple local dips via multidirectional component analysis: IEEE Transactions on Geoscience and Remote Sensing, **57**, 2798–2810, doi: 10.1109/TGRS.2018.2877702.

Cary, P. W., and C. Zhang, 2009, Ground roll attenuation with adaptive eigenimage filtering: 79th Annual International Meeting, SEG, Expanded Abstracts, 3302–3306, doi: 10.1190/1.3255545.

Chen, K., and M. D. Sacchi, 2015, Robust reduced-rank filtering for erratic seismic noise attenuation: Geophysics, **80**, no. 1, V1–V11, doi: 10.1190/geo2014-0116.1.

Freire, S. L. M., and T. J. Ulrych, 1988, Application of singular value decomposition to vertical seismic profiling: Geophysics, **53**, 778–785, doi: 10.1190/1.1442513.

Gan, S. W., Y. K. Chen, S. H. Zu, S. Qu, and W. Zhong, 2015, Structure-oriented singular value decomposition for random noise attenuation of seismic data: Journal of Geophysics and Engineering, **12**, 262–272, doi: 10.1088/1742-2132/12/2/262.

Gao, J. H., J. Mao, W. S. Man, W. C. Chen, and Q. Q. Zheng, 2006, On the denoising method of prestack seismic data in wavelet domain: Chinese Journal of Geophysics, **49**, 337–347, doi: 10.1002/cjg2.843.

Gao, J. J., M. D. Sacchi, and X. H. Chen, 2013, A fast reduced-rank interpolation method for prestack seismic volumes that depend on four spatial

dimensions: Geophysics, **78**, no. 1, V21–V30, doi: 10.1190/geo2012-0038.1.
Haggar, A. M., J. P. Windham, D. A. Reimann, D. O. Hearshen, and J. W. Froelich, 1989, Eigenimage filtering in MR imaging — An application in the abnormal chest wall: Magnetic Resonance in Medicine, **11**, 85–97, doi: 10.1002/mrm.1910110108.
Hassanpour, H., A. Zehtabian, and S. J. Sadati, 2012, Time domain signal enhancement based on an optimized singular vector denoising algorithm: Digital Signal Processing, **22**, 786–794, doi: 10.1016/j.dsp.2012.03.009.
Huang, W. L., R. Q. Wang, Y. K. Chen, H. J. Li, and S. W. Gan, 2016, Damped multichannel singular spectrum analysis for 3D random noise attenuation: Geophysics, **81**, no. 4, V261–V270, doi: 10.1190/geo2015-0264.1.
Huo, S. D., Y. Luo, and P. G. Kelamis, 2012, Simultaneous sources separation via multidirectional vector-median filtering: Geophysics, **77**, no. 4, V123–V131, doi: 10.1190/geo2011-0254.1.
Jeng, Y., Y. W. Li, C. S. Chen, and H. Y. Chien, 2009, Adaptive filtering of random noise in near-surface seismic and ground-penetrating radar data: Journal of Applied Geophysics, **68**, 36–46, doi: 10.1016/j.jappgeo.2008.08.013.
Jia, Y. N., S. W. Yu, L. N. Liu, and J. W. Ma, 2016, A fast rank-reduction algorithm for three-dimensional seismic data interpolation: Journal of Applied Geophysics, **132**, 137–145, doi: 10.1016/j.jappgeo.2016.06.010.
Lin, Y., and J. H. Zhang, 2020, Progressive denoising of seismic data via robust noise estimation in dual domains: Geophysics, **85**, no. 1, V99–V118, doi: 10.1190/geo2019-0010.1.
Liu, G. C., X. H. Chen, J. Du, and K. L. Wu, 2012, Random noise attenuation using f-x regularized nonstationary autoregression: Geophysics, **77**, no. 2, V61–V69, doi: 10.1190/geo2011-0117.1.
Liu, Y., and B. X. Li, 2018, Streaming orthogonal prediction filter in the t-x domain for random noise attenuation: Geophysics, **83**, no. 4, F41–F48, doi: 10.1190/geo2017-0322.1.
Liu, Z., J. W. Ma, and X. S. Yong, 2019, Line survey joint denoising via low-rank minimization: Geophysics, **84**, no. 1, V21–V32, doi: 10.1190/geo2018-0141.1.
Moreau, L., L. Stehly, P. Boue, Y. Lu, E. Larose, and M. Campillo, 2017, Improving ambient noise correlation functions with an SVD-based Wiener filter: Geophysical Journal International, **211**, 418–426, doi: 10.1093/gji/ggx306.
Oropeza, V., and M. Sacchi, 2011, Simultaneous seismic data denoising and reconstruction via multichannel singular spectrum analysis: Geophysics, **76**, no. 3, V25–V32, doi: 10.1190/1.3552706.
Porsani, M. J., M. G. Silva, P. E. M. Melo, and B. Ursin, 2010, SVD filtering applied to ground-roll attenuation: Journal of Geophysics and Engineering, **7**, 284–289, doi: 10.1088/1742-2132/7/3/007.
Porsani, M. J., B. Ursin, M. G. Silva, and P. E. M. Melo, 2013, Dip-adaptive singular-value decomposition filtering for seismic reflection enhancement: Geophysical Prospecting, **61**, 42–52, doi: 10.1111/j.1365-2478.2012.01059.x.
Tian, Y. A., Y. Li, and B. J. Yang, 2014, Variable-eccentricity hyperbolic-trace TFPF for seismic random noise attenuation: IEEE Transactions on Geoscience and Remote Sensing, **52**, 6449–6458, doi: 10.1109/TGRS.2013.2296603.
Trickett, S., 2002, F-x eigenimage noise suppression: 72nd Annual International Meeting, SEG, Expanded Abstracts, 2166–2169, doi: 10.1190/1.1567245.
Trickett, S., 2008, F-xy Cadzow noise suppression: 78th Annual International Meeting, SEG, Expanded Abstracts, 2586–2590, doi: 10.1190/1.3063880.
Vrabie, V. D., J. I. Mars, and J. L. Lacoume, 2004, Modified singular value decomposition by means of independent component analysis: Signal Processing, **84**, 645–652, doi: 10.1016/j.sigpro.2003.12.007.
Wang, X. J., B. H. Wen, and J. W. Ma, 2019, Denoising with weak signal preservation by group-sparsity transform learning: Geophysics, **84**, no. 6, V351–V368, doi: 10.1190/geo2019-0063.1.
Yu, S. W., and J. W. Ma, 2018, Complex variational mode decomposition for slop-preserving denoising: IEEE Transactions on Geoscience and Remote Sensing, **56**, 586–597, doi: 10.1109/TGRS.2017.2751642.
Zhang, C., and M. van der Baan, 2018, Multicomponent microseismic data denoising by 3D shearlet transform: Geophysics, **83**, no. 3, A45–A51, doi: 10.1190/geo2017-0788.1.
Zhang, C., and M. van der Baan, 2019, Strong random noise attenuation by shearlet transform and time-frequency peak filtering: Geophysics, **84**, no. 6, V319–V331, doi: 10.1190/geo2018-0500.1.
Zhang, D., Y. T. Zhou, H. M. Chen, W. Chen, S. H. Zu, and Y. K. Chen, 2017, Hybrid rank-sparsity constraint model for simultaneous reconstruction and denoising of 3D seismic data: Geophysics, **82**, no. 5, V351–V367, doi: 10.1190/geo2016-0557.1.

Biographies and photographs of the authors are not available.